J Mater Sci (2009) 44:4546–4552
DOI 10.1007/s10853-009-3689-z

Nanostructure formation in the surface layer of metals under influence of high-power electric current pulse

A. Vinogradov · A. Mozgovoi · S. Lazarev · S. Gornostai-Polskii · R. Okumura · S. Hashimoto

Received: 9 April 2009 / Accepted: 15 June 2009 / Published online: 1 July 2009

Abstract The possibility to tailor the microstructure of metals is explored utilising a skin-effect for surface treatment. The theoretical simulation of the electric and magnetic fields in a metallic cylinder shows that melting followed by rapid quenching can occur in a skin layer of 5–10-μm thickness if the amplitude of a single electric pulse of several nanoseconds duration is of the order of hundreds kiloamperes. The experiments using the SUS304 stainless steel show that besides a thin amorphous layer, a specific nano-twin structure can form at the near-surface region. The appearance of nano-twins is explained considering the stress components arising at the surface layer and in the bulk of the specimen during shock wave propagation caused by temperature gradients and the Lorentz force. It is shown that the high stress amplitudes can arise locally, furnishing the required conditions for twin nucleation and resulting in intensive plastic deformation of the sub-surface layer.

Introduction

Many physical and mechanical properties of materials depend strongly on the surface state. For instance, hardness, fatigue life and wear resistance benefit from surface strengthening which can be achieved in a variety of techniques including severe plastic deformation, plating, ion implantation, laser irradiation, etc. The ultimate properties have been achieved in materials in their nano- and amorphous states [1]. Both nano- and amorphous structures are commonly obtained in metals from melts of very specific chemical compositions by utilising a variety of rapid quenching techniques where a rather high critical cooling rate of 10^5–10^7 K/s is achieved as required for amorphisation. At lower quenching rates, ordinary crystallisation or formation of ultrafine grain or nano-structure is observed with characteristic grain dimensions from few nanometres to few hundred nanometres, respectively. Numerous rapid quenching techniques allow obtaining thin films, ribbons, flakes and powders of micrometre dimensions [2]. In contrast, severe plastic deformation is capable of producing bulk articles with the ultrafine grain and nano-structure [3].

In this study, we explore the possibility to create novel microstructures by combining both rapid quenching and severe plastic deformation. We make use of a skin-effect in conductors, arising from the short electric current pulse flowing through the conductor, for their surface heating up to melting followed by rapid cooling due to heat transfer the bulk. It was supposed that various ultrafine grain, nano- and even amorphous structures can be produced in the surface layer of metals in this way [4]. The first theoretical attempt has been made in ref. [4] to simulate the behaviour of the electric and magnetic fields in a metallic cylinder subject to a rapid discharge of a bank of capacitors as shown schematically in Fig. 1. It was demonstrated that melting followed by rapid quenching can occur in a skin layer of 5–10-μm thickness if the amplitude of the passing electric pulse of several nanoseconds duration is high enough, i.e. of the order of 10^2 kA. Furthermore, it appeared that since solidification of the molten layer occurs within a microsecond or sub-microsecond time

A. Vinogradov (✉) · S. Hashimoto
Osaka City University, Osaka 558-8585, Japan
e-mail: alexei@imat.eng.osaka-cu.ac.jp

A. Mozgovoi · S. Lazarev · S. Gornostai-Polskii · R. Okumura
Institute of Experimental Physics, Sarov 607190, Russia

Present Address:
R. Okumura
Materials Engineering Department, Denso Corp.,
Kariya 448-8661, Japan

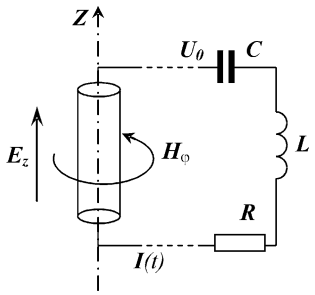

Fig. 1 Schematic diagram of the problem and experimental setup

scale, very high quenching rates of 10^8–10^9 K/s are achievable, providing an appealing novel opportunity for amorphisation or significant modification and nano-structurisation of the surface layer in conductors. The possibility to obtain thickness of 5–10 μm amorphous layer in the commercial SUS304 stainless steel was then successfully demonstrated by the same authors [5], which agrees with common estimates of the skin layer thickness [6]. Theoretical calculations in this study show that the extremely high stresses may arise from the temperature gradients and Lorenz force action resulting in intensive plastic deformation of the sub-surface layer. The experiments under this study utilising an ultra-high power generator producing a short electric current pulse flowing through copper or SUS304 stainless steel cylindrical specimens reveal that a specific nano-twin structure can be formed in the surface layer and in the bulk of the specimens depending on the electric pulse parameters. The appearance of nano-twins is explained from the theoretical consideration of the stress components arising at the surface vicinity and in the bulk of the specimen.

Use of skin-effect for surface heating, melting and rapid quenching

Let us consider an endless conducting cylinder with the symmetry axis Z in a circuit shown in Fig. 1. The procedure, which allows evaluating the parameters of the external circuit such as the resistance R, capacitance C, inductance L and the initial voltage U_0, as well as the dimensions of the metallic cylinder l and r_0, is given in [4] to ensure melting and rapid quenching in the surface layer.

The initial system of differential equations describing a given problem can be written in a classic Maxwell's form for the electric $\boldsymbol{E}$ and magnetic $\boldsymbol{H}$ fields together with a heat transfer equation:

$$\begin{aligned} \nabla \times \mathbf{H} &= \frac{1}{\rho}\mathbf{E}, \\ \nabla \times \mathbf{E} &= -\mu_a \frac{\partial \mathbf{H}}{\partial t}, \\ \rho_m c_V \frac{\partial T}{\partial t} &= \nabla \cdot (k \nabla T) + \frac{1}{\rho}|\mathbf{E}|^2, \end{aligned} \tag{1}$$

where the right-hand side of the last equation includes the Joule heating term proportional to $|\mathbf{E}|^2$ as a heat source. Here, ρ_m is the materials density, μ_a is the magnetic permeability, c_V is the specific heat capacity and k is the heat conductivity of the material. Apparently, the system of equations (1) should be completed with the ordinary electric equations for the external circuit given as

$$\begin{aligned} L\frac{\mathrm{d}I}{\mathrm{d}t} + RI - U(t) + lE_z(t, r_0) &= 0, \\ \frac{\mathrm{d}U}{\mathrm{d}t} &= -\frac{I(t)}{C}, \end{aligned} \tag{2}$$

with initial conditions setting the initial discharge voltage U_0

$$U(0) = U_0, \quad I(0) = 0. \tag{3}$$

In order to model the dynamics of various processes in the actual experimental installation utilising the electrical energy of the bank of capacitors discharging on a low-inductance load, the system of equations (2) and (3) was solved together. The details of the problem formulation and solution have been reported in [4, 5]. For instance, for a copper cylinder having the length $l = 10$ mm and radius $r_0 = 0.1$–0.5 mm at $T_0 = 300$ K, $C = 0.1$ μF, $R = 0.3$ Ohm, $L = 5$ nHn and $U_0 = 100$ kV, the peak current magnitude reaches 180–250 kA while the pulse duration is as short as 40–50 ns. The maximum thickness of the molten layer R_m was found to be 10 μm, and the melting time was 230 ns. Cooling until complete solidification occurred within approximately 1 μs. The maximum temperature on the surface reached almost 2,000 K, which is between the melting point $T_m = 1{,}356$ K and vaporization temperature $T_v = 2{,}868$ K. The maximum quenching rate, $\partial T/\partial t$, was of 2×10^8 K s^{-1}. This quenching rate is still not enough for amorphisation of pure metals; it is, however. within the range of typical quenching rates attained in melt-spinning techniques used for production of a broad variety of amorphous alloys [2]. Using the model constituted by Eqs. 1 and 3, one can show that the depth of the molten layer varies in a range of 0.1–40 μm, depending on the specimen dimensions and initial voltage provided that the parameters of the experiment have been the realistically chosen [4, 5]. Hence, utilising a high-power generator described briefly in [7], which was modified to fit the cylindrical specimens of 1-mm diameter, the proposed scheme vas validated using Cu and SUS304 stainless steel. It was demonstrated that formation of the amorphous (glassy-like) layer in the intimate proximity (from zero to about 30 μm depending on the initial voltage U_0) to a free surface of the SUS304 steel (Fe–18Cr–8Ni) is possible after melting followed by rapid quenching caused by the short high power electric pulse. For this study, the most interesting finding reported in ref. [4] is that a specific twin structure is formed in the subsurface layer,

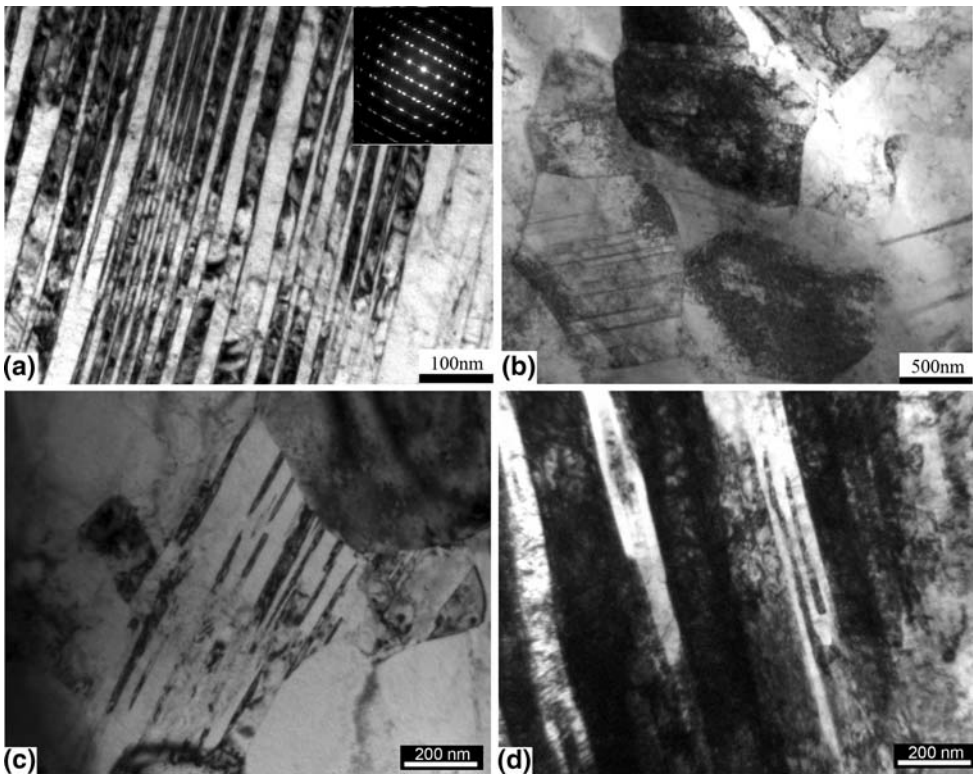

Fig. 2 Nano-scaled twin structure below the surface of a "skin-" treated SUS304 stainless steel **a** 25 μm below the surface; SEADP is indicative of the twinned structure; **b** 100 μm below the surface; **c** and **d** 100 μm below the surface. The initial discharge voltage is 70 kV (**a**, **b**) and 90 kV (**c**, **d**), respectively

extending up to 100 μm inside the material from the surface as illustrated in Fig. 2 (the details of experimental procedure, specimen preparation and observation can be found in [5]). Transmission electron microscopy (TEM) with the selected area electron diffraction pattern (SAEDP) analysis reveals that this structure differs drastically from that is commonly found in the bulk of the as-received specimens. After the 'skin' treatment, the structure near the surface consists primarily of regions which are multiply twinned along {111} planes with the nanometre scale twin spacing. The very fine twin lamellae, parallel to each other can be readily found here and there in TEM foils. Apparently, the density of twin population reduces with depth from the surface, c.f. Fig. 2a–d. Figure 2b shows that the twins in the bulk of the specimen are limited to the initial grain size which is of the order of 2–3 μm. The appearance of such a very fine nano-scaled twin structure, induced by the 'skin' treatment, is difficult to explain by annealing-type effects caused by the temperature rise at the specimen surface due to the skin electric current. Since the cooling rate has been proven very high [4, 5], the time interval over which the surface layer is exposed to the high temperature influence is too short to facilitate diffusion processes controlling the annealing effects. Besides, the twin structure appearance does not resemble typical annealing twin patterns, for example [8]. On the other hand, it is well known that the fine twin lamellae with the nano-scale spacing can be produced mechanically at high stresses due to plastic deformation [9–11]. Appearance of mechanical twins assumes two factors of primary importance: (i) high stresses approaching a sizable fraction of the theoretical cohesive strength $\tau \propto \mu/10$ with μ—shear modulus of the material, (ii) impeded alternative accommodative mechanisms such as dislocation motion. In the course of conventional plastic deformation, the dislocation motion can be blocked by high internal stresses arising from dislocation accumulation during strain hardening. In the experiments under this study, the dislocation motion is limited due to a very short influence from the electric pulse. The mechanical twins form very fast, with the velocity of sound [10] and can be highly possible candidates for alternative sources of plastic deformation. Therefore, the internal stresses arising from the influence of electric and magnetic fields during the "skin" treatment of the metal surface should be evaluated to shed light on the feasibility of twin nucleation. This will be accomplished in the next section.

Stress calculation

Problem statement

The pressure caused by the electromagnetic field acting on the specimen in the geometry shown in Fig. 1 is proportional to the Pointing vector, i.e. to the vector product

$\boldsymbol{E} \times \boldsymbol{H}$. The displacement vector $\boldsymbol{U}$, will have both axial and radial components $\boldsymbol{U} = \{U_r, 0, U_z\}$.

In order to calculate the stresses which arise in the metallic specimen when the high power electric pulse is passing through, the equation for the vector $\boldsymbol{U}$ should be added to the system of Maxwell equations for electric and magnetic vectors. The equation describing the mechanical behaviour of an isotropic deforming media is written as

$$\rho_m \frac{\partial^2 \mathbf{U}}{\partial t^2} = \nabla \cdot [\boldsymbol{\sigma}] + \mathbf{F}, \tag{4}$$

where the Lorentz force term and the linear isotropic expansion term are incorporated in the right hand side; $[\boldsymbol{\sigma}]$ is the stress tensor, $\boldsymbol{F}$ is the net bulk force vector. In the axially symmetrical case the stress tensor takes a form

$$[\boldsymbol{\sigma}] = \begin{pmatrix} \sigma_r & 0 & \sigma_{rz} \\ 0 & \sigma_\varphi & 0 \\ \sigma_{zr} & 0 & \sigma_z \end{pmatrix}, \tag{5}$$

with the components given as

$$\begin{pmatrix} \sigma_r \\ \sigma_\varphi \\ \sigma_z \\ \sigma_{rz} \end{pmatrix} = \lambda \begin{pmatrix} \frac{1-v}{v} & 1 & 1 & 0 \\ 1 & \frac{1-v}{v} & 1 & 0 \\ 1 & 1 & \frac{1-v}{v} & 0 \\ 0 & 0 & 0 & \frac{1-2v}{v} \end{pmatrix} \begin{pmatrix} \varepsilon_r - \alpha_T(T - T_0) \\ \varepsilon_\varphi - \alpha_T(T - T_0) \\ \varepsilon_z - \alpha_T(T - T_0) \\ \varepsilon_{rz} \end{pmatrix} \tag{6}$$

Components of the strain tensor $[\boldsymbol{\varepsilon}]$ are given as:

$$\varepsilon_r = \frac{\partial U_r}{\partial r},\ \varepsilon_\varphi = \frac{U_r}{r},\ \varepsilon_z = \frac{\partial U_z}{\partial z},\ \varepsilon_{rz} = \frac{1}{2}\left(\frac{\partial U_r}{\partial z} + \frac{\partial U_z}{\partial r}\right). \tag{7}$$

Hence, the initial system of equations takes a form:

$$\begin{aligned}
&\nabla \times \mathbf{H} = \frac{1}{\rho}\mathbf{E}, \\
&\nabla \times \mathbf{E} = -\mu_a \frac{\partial \mathbf{H}}{\partial t}, \\
&\rho_m c \frac{\partial T}{\partial t} = \nabla \cdot (k \nabla T) + \frac{1}{\rho}|\mathbf{E}|^2, \\
&\rho_m \frac{\partial^2 \mathbf{U}}{\partial t^2} = (\lambda + 2\mu)\nabla(\nabla \cdot \mathbf{U}) - \mu \nabla \times (\nabla \times \mathbf{U}) \\
&\qquad - \alpha_T K \nabla T + \mu_a \frac{1}{\rho} \cdot \mathbf{E} \times \mathbf{H}\,, \\
&\mu = \frac{E_u}{2(1+v)}, \quad \lambda = \frac{E_u v}{(1+v)(1-2v)}, \quad K = \frac{E_u}{3(1-2v)}.
\end{aligned} \tag{8}$$

Here, E_u, μ and K are the Young's, shear and bulk moduluses, respectively, v is the Poisson ratio, $\boldsymbol{\varepsilon}_{ij}$ are the strain tensor components, U_r, U_z are the displacement vector components, α_T is the linear heat expansion coefficient and λ is the Lame constant. The right-hand side of the third equation includes the Joule heating term proportional to $|\mathbf{E}|^2$ as a heat source. The system is said to be thermally isolated because the energy losses due to irradiation have been proven negligible [4].

Using Raleigh damping, which is commonly used to provide a source of energy dissipation in analyses of structures responding to dynamic loads and having $\mathbf{H} = \{0, H, 0\}$, $\mathbf{E} = \{E_r, 0, E_z\}$ and $\mathbf{U} = \{U_r, 0, U_z\}$, the equations (8) in cylindrical coordinates $\{r, z\}$ take a final form:

$$\begin{aligned}
&\mu_a \frac{1}{\rho}\frac{\partial H_\varphi}{\partial t} = \frac{1}{r}\left(r\frac{\partial^2 H_\varphi}{\partial r^2} + \frac{\partial H_\varphi}{\partial r} - \frac{H_\varphi}{r}\right) + \frac{\partial^2 H_\varphi}{\partial z^2}, \\
&E_z = \frac{\rho}{r}\frac{\partial}{\partial r}(rH_\varphi), \quad E_r = -\rho\frac{\partial H_\varphi}{\partial z}, \\
&\rho_m c \frac{\partial T}{\partial t} = k\left(\frac{\partial^2 T}{\partial r^2} + \frac{\partial^2 T}{\partial z^2}\right) + \frac{k}{r}\frac{\partial T}{\partial r} + \frac{1}{\rho}\left(E_r^2 + E_z^2\right), \\
&\rho_m \frac{\partial^2 U_r}{\partial t^2} = (\lambda + 2\mu)\left(\frac{\partial^2 V_r}{\partial r^2} + \frac{\partial}{\partial r}\left(\frac{V_r}{r}\right)\right) \\
&\qquad + \mu\frac{\partial^2 V_r}{\partial z^2} + (\lambda + \mu)\frac{\partial^2 V_z}{\partial r \partial z} \\
&\qquad - \frac{\mu_a}{\rho}E_z H_\varphi - \alpha_T K \frac{\partial T}{\partial r} + \alpha_R \rho_m \frac{\partial U_r}{\partial t}, \\
&\rho_m \frac{\partial^2 U_z}{\partial t^2} = (\lambda + 2\mu)\frac{\partial^2 V_z}{\partial z^2} + \mu\left(\frac{\partial^2 V_z}{\partial r^2} + \frac{1}{r}\frac{\partial V_z}{\partial r}\right) \\
&\qquad + (\lambda + \mu)\left(\frac{\partial^2 V_r}{\partial r \partial z} + \frac{1}{r}\frac{\partial V_r}{\partial z}\right) \\
&\qquad + \frac{\mu_a}{\rho}E_r H_\varphi - \alpha_T K \frac{\partial T}{\partial z} + \alpha_R \rho_m \frac{\partial U_z}{\partial t}, \\
&V_r = U_r + \beta_R \frac{\partial U_r}{\partial t}, \quad V_z = U_z + \beta_R \frac{\partial U_z}{\partial t}.
\end{aligned} \tag{9}$$

where, U_r and U_z are the radial and axial components of the displacement vector $\boldsymbol{U}$, respectively, and α_R and β_R are the coefficients of Raleigh damping, which are commonly expressed as

$$\alpha_R = 4\pi\xi\frac{f_{\min} f_{\max}}{f_{\min} + f_{\max}}, \quad \beta_R = \frac{\xi}{\pi(f_{\min} + f_{\max})}, \tag{10}$$

where ξ is the damping efficiency ranging between 0 and 1, $f_{\min}$ and $f_{\max}$ stand for the lower and upper frequency in the working frequency range, respectively. For numeric calculations, $f_{\min}$ and $f_{\max}$ are chosen as 0.5 an 90 MHz, respectively.

Initial and boundary conditions are set as

$$\begin{aligned}
&H_\varphi(0, r, z) = 0, \qquad U_z(0, r, z) = 0, \quad U_r(0, r, z) = 0, \\
&H_\varphi(t, r_0) = \frac{I(t)}{2\pi r_0}, \quad T(0, r, z) = T_0, \\
&\left.\frac{\partial T}{\partial r}\right|_{r=0} = 0, \quad \left.\frac{\partial T}{\partial r}\right|_{r=r_0} = 0, \quad \left.\frac{\partial E_z}{\partial r}\right|_{r=0} = 0
\end{aligned} \tag{11}$$

The free surface state determines boundary conditions for U_z and U_r in the Lame equation on the surface of the specimen:

$$\sigma_r|_{y=r_0} = (2\mu+\lambda)\frac{\partial U_r}{\partial r} + \lambda\left(\frac{\partial U_z}{\partial z} + \frac{U_r}{r}\right) = 0,$$
$$\sigma_\varphi|_{y=r_0} = (2\mu+\lambda)\frac{U_r}{r} + \lambda\left(\frac{\partial U_z}{\partial z} + \frac{\partial U_r}{\partial r}\right) = 0, \quad (12)$$
$$\sigma_z|_{y=r_0} = (2\mu+\lambda)\frac{\partial U_z}{\partial z} + \lambda\left(\frac{\partial U_r}{\partial r} + \frac{U_r}{r}\right) = 0.$$

The boundary conditions on the Z axis in the centre of the specimen ($r = 0$) take a form (due to the axial symmetry):

$$U_r(t,0,z) = 0, \quad \left.\frac{\partial U_z}{\partial r}\right|_{t,r=0,z} = 0. \quad (13)$$

Thus, together with Eqs. 2 and 3, the problem is fully defined and can be solved numerically.

Numerical estimates and discussion

Equations 6, 7, 9 and10 were solved together with electric equations (2) and initial and boundary conditions (3, 11–13). Numeric solutions were obtained using finite element method within a mesh constructed in r-z space having 1440 elements and 794 nodes. The Lagrange polynomial functions of the second order were taken for approximations.

For illustrative purposes, the calculations of internal stresses caused by high-power short electric pulse passing through a conductive material have been performed for Cu cylinder of $r_0 = 0.5$-mm initial radius and 5-mm length (regretfully, for the SUS304 steel, only few required material constants are known, which makes it impossible to perform quantitative modelling). All the other conditions were set the same as in [4], i.e. $T_0 = 300$ K, $C = 0.1$ μF, $R = 0.3$ ohm, $L = 5$ nH and $U_0 = 100$ kV. Figures 3 and 4 show the cumulative von Mises stresses arising from the linear thermal expansion and Lorentz force components

$$\sigma_{\text{Von-Mises}} = \sqrt{\sigma_r^2 + \sigma_\theta^2 + \sigma_z^2 - \sigma_r\sigma_\theta - \sigma_r\sigma_z - \sigma_\theta\sigma_z + 3\sigma_{rz}^2} \quad (14)$$

and its components calculated in cylindrical coordinates (r, θ, z) for $r = 0$ (specimen axis) and $r = 0.5$ mm (specimen surface) in the middle of the specimen $z = 2.5$ mm. The shock-wave character of the stress temporal and spatial distribution is evident, particularly in Fig. 5, where the snapshots of the axial component of von Mises stresses distribution over the specimen are shown in subsequent instants of time. The shock wave propagates from the surface to the bulk and back in an oscillating manner with attenuation caused by Raleigh damping introduced in Eqs. 9. The duration of wave propagation depends on materials' properties and may vary from several microseconds to several milliseconds which is quite enough to activate subsonic or even trasonic dislocation motion and mechanical twinning, which can be viewed as a cooperative motion of several partial dislocations. While the σ_{rz} component is negligible both at the surface and in the bulk, the radial σ_r and axial σ_z and σ_φ components may attain very high peak magnitudes of several gigapascals, which is not unexpected for shock wave loading. The average magnitude of stress components near the surface is notably higher than that in the bulk which accounts for the higher possibility to find the twinned domains in the surface proximity, i.e. decreasing twin density with the depth from the surface.

Gerland et al. [12] used a surface treatment with shock waves caused by explosion in a thin layer applied to a 316L stainless steel. Similar to the results in this study, the near surface structure was found to be composed of mechanical

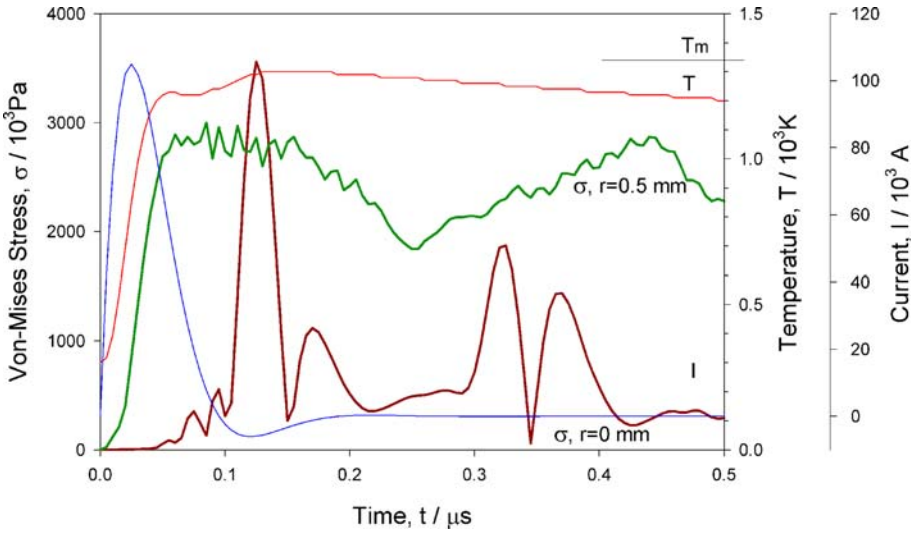

Fig. 3 Cumulative von Mises stress on the axis $r = 0$ and on the surface $r = 0.5$ mm of Cu cylinder subjected to the influence of the ultrahigh power short electric current pulse. The electric current magnitude I and surface temperature T are plotted for comparison and time scaling. T_m—melting temperature

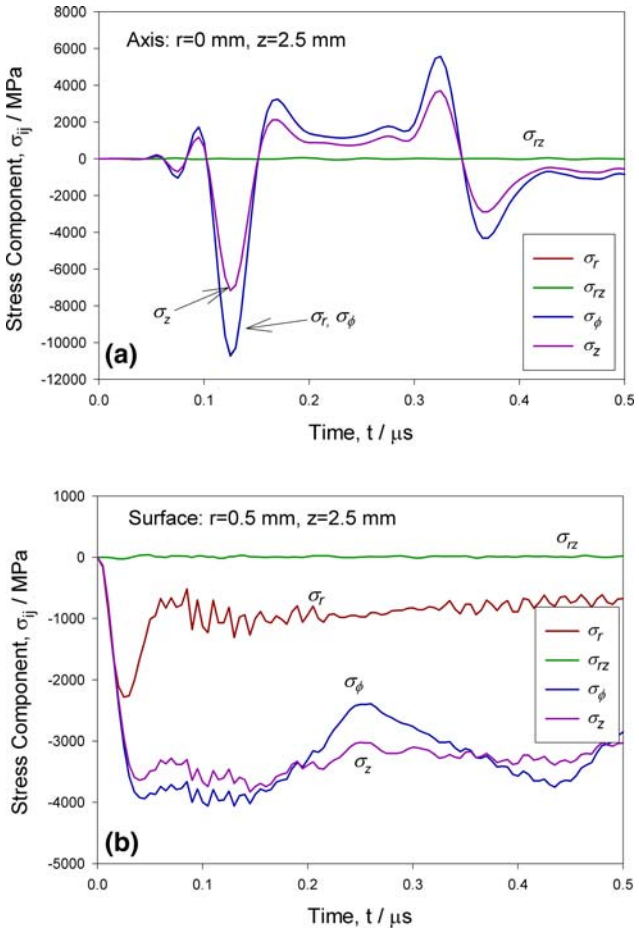

Fig. 4 Stress–tensor components (normal and shear) on the axis (**a**) and on the surface (**b**) of Cu cylinder subjected to the influence of the ultrahigh power short electric current pulse

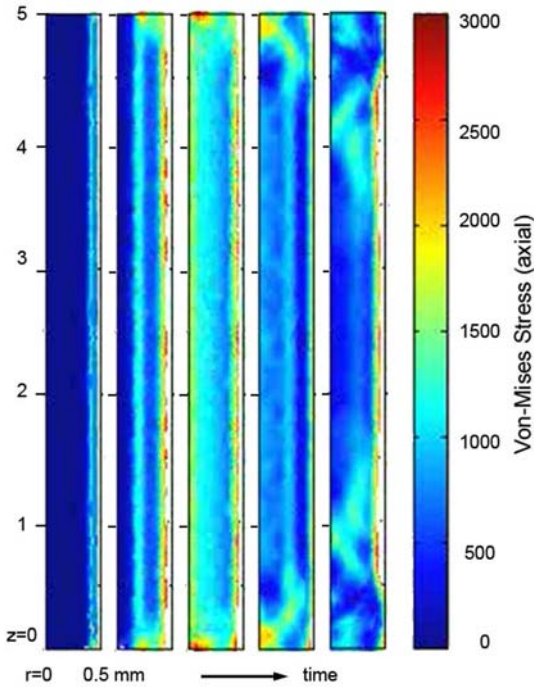

Fig. 5 Snapshots showing the von Mises stress distribution over the cylindrical specimen of 0.5-mm radius and 5-mm length in subsequent instants of time

twins, the density of which decreased with increasing depth. Firrao et al. [13] have also shown that mechanical twins are readily formed in the 304 stainless steel subjected to stress impact caused by explosions of small charges in the surface vicinity. The benefits for the mechanical properties of the nanostructured steels produced by explosion influence is argued in [12, 13]. Ample evidence exists in the literature showing twin formation due to severe plastic deformation caused by intense ultrasonic shot peening [14], mechanical attrition [15] or shock pulse loading [16]. The minute mechanisms of twin formation under shock wave loading have yet to be explored, possibly with the help of atomistic molecular dynamic simulations in a way similar to those performed in [17]. The results of this study may serve as a starting point for further quantitative modelling. They suggest that the high local stress conditions required for twin nucleation in the surface layer are fulfilled. Indeed, assuming the shear stress required for twin nucleation given as [18]

$$\tau \approx \frac{\gamma^{\mathrm{SFE}}}{b_1}, \tag{15}$$

where γ^{SFE} is the stacking fault energy and $b_1$is the Burgers vector of the twinning dislocation $b_1 = \frac{a}{6}\langle 121\rangle$ for an f.c.c. crystal with a—lattice parameter, and taking γ^{SFE} for the 304 Fe–Cr–Ni steel of 17 mJ/m^2 [19], one estimates $\tau \approx 0.12$ GPa, which is notably smaller than the possible peak values of stress components in elastic waves arising in the body due to the 'skin' treatment by a high-power electric pulse. Furthermore, twinning can be plausibly expected in the materials with much higher stacking fault energy under the same treatment conditions.

Significant changes in the microstructure of skin-treated specimens and the formation of twin colonies in the subsurface layer suggest that macrocharacteristics of treated metals may alter considerably. The Vickers microhardness HV was measured using a Shmiadzu dynamic Ultra-hardness tester DUH-1 at 20-g load and 20-s exposure time. Ten to twenty measurements along the specimen gauge part were averaged. The depth of indentation did not exceed 2–3 μm. The HV values in the specimens subjected to 'skin' treatment with the capacitor discharge from 70, 75 and 80 kV are found to be of 200 ± 23 HV, 161 ± 25 HV and 140 ± 27, respectively. All these values are notably higher than that for the reference of the "as-received" SUS304 sample—124 ± 6 HV, which is consistent with formation of the hardened twin nano-structure in the surface

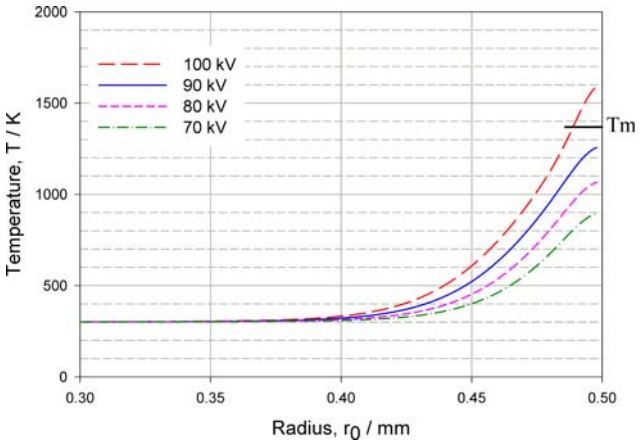

Fig. 6 Solutions of Eqs. 8 and 2 showing temperature profiles in the subsurface layer of Cu cylinder of 0.5-mm radius and 10-mm length after 0.4 μs since the capacitor discharge from different initial voltages. T_m—melting temperature

layer. Interestingly, that discharging capacitors from smaller voltage (70 kV) results in the highest hardness of the surface layer which agrees with microstructural observations: populations of twins are easier to see in the 70-kV-treated specimens while the density of twins reduces with increasing voltage (this has been noticed earlier in ref. [5]). Furthermore, this is also consistent with numeric evaluation of the temperature profile in the subsurface layer, Fig. 6: the thickness of the heated layer is found to be typically of the order of 100 μm almost independently of the discharge voltage, which is considerably wider than the skin layer (50–10 μm). However, the maximum temperature reached in the proximate vicinity of surface reduces sharply with voltage reduction. Even though this temperature reduces very quickly as we have discussed above (see [5] for details), this can be another argument why the nano-twin structure is more clearly seen after discharge from 70 kV.

One can notice in Fig. 5 that maximum von Mises stresses are obtained in the shock-wave within the 100-μm sub-surface layer, being in accordance with TEM observations showing that twin colonies are readily observed in the subsurface region up to about a 100-μm thickness, whereas they are rarely or not at all observed in the bulk of the specimen. Although, the only qualitative comparison between the results of calculations and structural observations are still possible, a fair agreement is seen between the numeric estimates, microstructural observations and microhardness assessment.

References

1. Gleiter H (1989) Progr Mater Sci 33:223
2. Beck H, Guntherodt H-J (eds) (1981) Glassy metals (topics in applied physics), vol 46. Springer, Germany
3. Valiev RZ, Islamgaliev RK, Alexandrov IV (2000) Progr Mater Sci 45:103
4. Vinogradov A, Lazarev SG, Mozgovoi AL, Hashimoto S (2005) Philos Mag Lett 85:575
5. Vinogradov A, Lazarev SG, Mozgovoi AL, Gornostai-Polskii SA, Okumura R, Hashimoto S (2007) J Appl Phys 101:033510–033510-7
6. Landau LD, Lifshitz EM (1984) Electrodynamics of continuous media, vol 8. Pergamon, Oxford, UK
7. Voronin VV, Tananakin VA, Pavlov SS, Tsiberev VP, Voronov SL (1977) In: Proceedings 11th IEEE international pulsed power conference, Baltimore, Maryland, USA, p 1566
8. Jones AR (1981) J Mater Sci 16:1374. doi:10.1007/BF01033854
9. Nartia N, Takamura J (1992) In: Nabarro FRN (ed) Dislocations in solids, vol 9. Elsevier, Amsterdam
10. Rigsbee JM, Benson RB (1977) J Mater Sci 12:406–409. doi:10.1007/BF00566284
11. Friedel J (1964) Dislocations. Pergamon Press, Oxford, UK
12. Gerland M, Presles HN, Mendez J, Dufour JP (1993) J Mater Sci 28:1551. doi:10.1007/BF00363348
13. Firrao D, Matteis P, Scavino G, Ubertalli G, Ienco MG, Pellati G, Piccardo P, Pinasco MR, Stagno E, Montanari R, Tata ME, Brandimarte G, Petralia S (2006) Mat Sci Eng A 424:23
14. Liu G, Wang SC, Lou XF, Lu J, Lu K (2001) Scripta Mater 44:1791
15. Zhang HW, Hei ZK, Liu G, Lu J, Lu K (2003) Acta Mater 51:1871
16. Bakalinskaya ND, Zubov VI, Nadezhdin GN, Petrov YuN, Svechnikov VI, Stepanov GV (1988) J Strength Mater 20:1205
17. Gumbsch P, Gao H (1999) Science 283:965
18. Hirth JP, Lotte J (1982) Theory of dislocations. Wiley, New York
19. Murr LE (1975) In: Herndan VA (ed) Interfacial phenomena in metals and alloys. Techbooks, Herndan